Tunnel magnetoresistive sensors with non-hysteretic resistance-magnetic field curves using noncollinear interlayer exchange coupling through RuFe spacers

Prabhanjan D. Kulkarni[*], and Tomoya Nakatani[**]

Research Center for Magnetic and Spintronic Materials, National Institute for Materials Science, 1-2-1 Sengen, Tsukuba, Ibaraki 305-0047, Japan

[*] Present address: Centre for Sensors Vision Technology and IT, Central Manufacturing Technology Institute, Bengaluru, Karnataka, India.

[**] Corresponding author: nakatani.tomoya@nims.go.jp

ABSTRACT

Magnetic stabilization of the ferromagnetic layers of magnetoresistive elements is a key technological requirement for highly sensitive and accurate magnetic sensors. Here, we report on a tunnel magnetoresistive (TMR) sensor wherein the free layer (FL) magnetization is stabilized by combining exchange bias, noncollinear interlayer exchange coupling through a RuFe spacer, and orange-peel ferromagnetic coupling. This method facilitates the stabilization of the FL magnetization over a wide range of noncollinear angles with respect to the pinning direction by controlling the composition of the RuFe spacer. Moreover, the uniaxial anisotropy induced in the FL by annealing plays an important role in the resistance–magnetic field (*R–H*) curve, which was studied both experimentally and through simulation. The TMR devices exhibited negligible hysteresis even in the major *R–H* loops, which is promising for magnetic field-sensing applications.

Controlling and stabilizing the magnetization directions of ferromagnetic (FM) layers are important for spintronic devices, such as magnetic memories and sensors. Exchange bias, interlayer exchange coupling (IEC), and magnetic anisotropy are key tools for achieving this function. The unidirectional exchange bias obtained in an antiferromagnet (AFM)/FM bilayer structure is used to pin the magnetization of the FM layer, referred to as the spin-valve structure.[1] IEC oscillates between AFM and FM couplings depending on the thickness of the nonmagnetic spacer for various materials, such as Cr, Cu, and Ru.[2–5] The AFM-IEC through Cu and Ru spacers is particularly important for giant magnetoresistance devices and synthetic antiferromagnet structure,[6] respectively. Further, the recently reported noncollinear IEC in Co/RuFe/Co, Co/RuCo/Co, and Co/IrFe/Co trilayer structures facilitates the control of the magnetization configuration of the Co layers at arbitrary angles by changing the composition and thickness of the RuFe, RuCo, and IrFe spacers.[7–10]

Magnetization stabilization is critical for tunnel magnetoresistance (TMR) magnetic sensors, which have recently attracted much attention because of their expanding applications and markets. For many applications, TMR sensors must exhibit an output voltage proportional to the strength of the magnetic field. This can be achieved by stabilizing the magnetization of the free layer (FL) along one direction (easy axis) and sensing the magnetic field along the orthogonal direction (hard axis); consequently TMR devices exhibit pseudo linear resistance–magnetic field (*R–H*) response curves.[11–14] Various methods have been developed to induce magnetic anisotropy in FL, such as shape anisotropy,[15] external bias magnetic field,[11] perpendicular magnetic anisotropy,[16,17] annealing-induced uniaxial anisotropy,[18,19] and exchange bias.[12,13,20,21]

Uniaxial anisotropy orthogonal to the pinning direction is induced by two-step annealing at two different temperatures under magnetic fields along orthogonal directions.

Because the typical anisotropy field of annealing-induced uniaxial anisotropy is a few mT or smaller, soft-magnetic FLs with uniaxial anisotropy are often used for high-sensitivity TMR sensors.[19,22] However, as pointed out by Wang et al.,[12] FLs with only uniaxial anisotropy are demagnetized into a multi-domain structure under a zero magnetic field. Consequently, the *R*–*H* curves of the TMR devices exhibit magnetic hysteresis, which is undesirable for magnetic sensors. Another sensor design where the FL is stabilized by unidirectional anisotropy (exchange bias) results in a single-domain state of FL magnetization, causing a considerably smaller magnetic hysteresis.[12,13,20,21] These sensors achieve an orthogonal magnetization configuration between the FL and reference layer (RL) using two AFM layers with different blocking temperatures processed by two-step annealing.

This study developed a TMR sensor stack where the FL magnetization is stabilized in the single domain state along a noncollinear direction with respect to the pinning direction. This was achieved by transferring the exchange bias through the noncollinear IEC via a RuFe spacer. By controlling the directions of the noncollinear IEC and annealing-induced uniaxial anisotropy, TMR sensors with linear *R*–*H* curves and negligible magnetic hysteresis can be obtained, which are considered to be suitable for magnetic sensing applications.

The core component of the present study is two Co layers magnetically coupled in a noncollinear configuration through a RuFe spacer. Nunn et al.[7] reported that the noncollinear IEC between the Co layers can be controlled by the composition and thickness of the RuFe spacer. For simplicity, the RuFe thickness was fixed at 1 nm, whereas the RuFe composition was varied by co-sputtering deposition from Ru and Fe targets. The composition of the RuFe film was measured using X-ray fluorescence spectroscopy.

First, to measure the magnetization angle between two Co layers separated by a RuFe spacer, we fabricated current-in-plane giant magnetoresistance (CIP-GMR) spin-valve

structures of thermally oxidized Si substrate/Ta (2)/Ru (2)/IrMn (6)/$Co_{50}Fe_{50}$ (1)/Co (2)/$Ru_{100-x}Fe_x$ (1)/Co (3)/Cu (3)/$Co_{90}Fe_{10}$ (5)/Ru (4) (thickness in nm), as shown in Fig. 1(a). The CIP-GMR films were annealed at 350 °C for 1 h under a magnetic field of 0.7 T to pin the magnetization direction of the $Co_{50}Fe_{50}$ (1)/Co (2) pinned layer (PL). The magnetization configuration diagram in Fig. 1(a) shows that the magnetization of the Co (3) RL was fixed at an angle of θ_{IEC} with respect to the PL magnetization by the noncollinear IEC through the RuFe spacer. The FL magnetization was saturated by an external magnetic field (H) of 5 mT applied at θ angle with respect to the PL magnetization. Figure 1(b) shows the θ dependence of the GMR ratio, defined as $(R - R_{\mathrm{min}})/R_{\mathrm{min}}$ (R_{min}: minimum resistance), of the spin-valve films with three different RuFe compositions. θ at (GMR ratio) = 0 corresponds to θ_{IEC}, which was 132°, 101°, and 77° for x = 57, 63, and 67 at. %, respectively. As shown in Fig. 1(c), θ_{IEC} varied as 50°–130° by changing x.

The noncollinear IEC can be phenomenologically described by bilinear and biquadratic IEC components, whose energies are expressed by J_1 and J_2, respectively. J_1 and J_2 are obtained by fitting the magnetization (M) vs. H curves (e.g., for the $Ru_{40}Fe_{60}$ spacer in the inset of Fig. 1(d)) by minimizing the total magnetic energy with Zeeman, IEC and exchange bias energies.

$$E_{\mathrm{total}} = E_{\mathrm{Z}} + E_{\mathrm{IEC}} + + E_{\mathrm{eb}}, \tag{1}$$

where

$$E_{\mathrm{Z}} = -H(M_{\mathrm{PL}}t_{\mathrm{PL}}\cos\varphi_{\mathrm{PL}} + M_{\mathrm{RL}}t_{\mathrm{RL}}\cos\varphi_{\mathrm{RL}} + M_{\mathrm{FL}}t_{\mathrm{FL}}\cos\varphi_{\mathrm{FL}}), \tag{2}$$

$$E_{\mathrm{IEC}} = -J_1\cos(\varphi_{\mathrm{PL}} - \varphi_{\mathrm{RL}}) - J_2\cos^2(\varphi_{\mathrm{PL}} - \varphi_{\mathrm{RL}}), \tag{3}$$

$$E_{\mathrm{eb}} = -J_{\mathrm{k}}\cos\varphi_{\mathrm{PL}}, \tag{4}$$

where M and t are the saturation magnetization and film thickness, respectively, φ is the angle

between M and H, and J_k is the exchange bias energy between the PL and the IrMn AFM layer. As shown in Fig. 1(d), J_2 exhibited similar values of –0.3 mJ/m^2 for x ranging as 54–70 at. %, whereas J_1 varied between negative and positive values, corresponding to AFM and FM bilinear IECs, respectively. As previously reported,[23,24] θ_{IEC} is determined using J_1 and J_2 as $\theta_{IEC} = \cos^{-1}(-J_1/2J_2)$ when $-2 \le J_1/J_2 \le 2$. The calculated θ_{IEC} were consistent with the directly measured values [Fig. 1(c)].

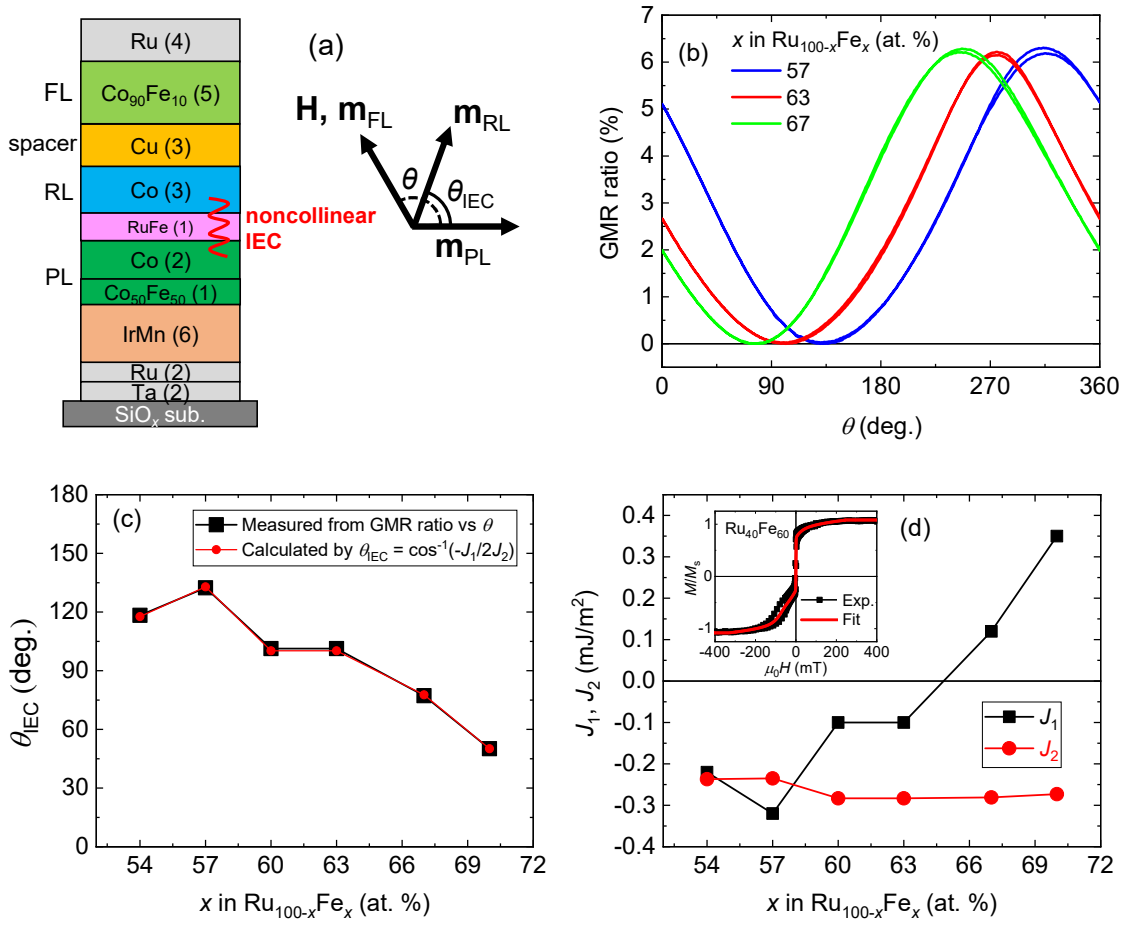

FIG.1. (a) Schematic layer structure and magnetization configuration of the CIP-GMR spin-valves with a noncollinear IEC between PL and RL through the $Ru_{100-x}Fe_x$ spacers. External magnetic field (5 mT) was applied at θ angle with respect to the PL magnetization ($\mathbf{m}_{PL}$). (b) GMR ratio vs. θ curves for x = 57, 63, and 67 at. %. The θ value at GMR ratio = 0 corresponds

to θ_{IEC}. x dependences of (c) θ_{IEC} and (d) J_1 and J_2. The inset of (d) shows the M–H curve for x = 60 at. % and its fitting curve.

Subsequently, we fabricated TMR spin-valve devices with a layer structure of thermally oxidized Si substrate/Cu bottom electrode/Ta (2)/Ru (2)/IrMn (6)/CoFe (1)/Co (2)/$Ru_{100-x}Fe_x$ (1)/Co (3)/AgSn (2.5)/CoFe (1)/CoFeBTa (30)/Ta (0.3)/CoFeB (3)/MgO (1.8)/CoFeB (2.5)/Ta (0.15)/CoFeB (0.5)/CoFe (1)/Ru (0.8)/CoFe (3)/IrMn (8)/Ru (8) (thickness in nm) with variations in the Fe concentration of the RuFe spacer including pure Ru, as shown in Fig. 2(a). The nominal compositions of the alloy layers were $Ir_{20}Mn_{80}$, $Co_{50}Fe_{50}$, $Ag_{90}Sn_{10}$, $Co_{38}Fe_{38}B_{19}Ta_5$, and $Co_{40}Fe_{40}B_{20}$. The magnetization of the Co (2) PL2 was pinned along the noncollinear direction with respect to that of CoFe (1)/Co (2) PL1. The CoFe (1)/CoFeBTa (30)/Ta (0.3)/CoFeB (3) layers functioned as FL through strong FM coupling between the CoFeBTa amorphous soft magnetic layer and the CoFeB electrode via the thin Ta layer, which was inserted to promote the crystallization of CoFeB during annealing. The AgSn spacer was inserted to weakly ferromagnetically couple the magnetizations of PL2 and FL via orange-peel coupling.[25,26] Thus, the direction and strength of the unidirectional stabilization field to the FL were controlled by the RuFe composition and AgSn thickness, respectively. The layers above the MgO barrier were patterned to a circular shape with a diameter of 40 μm, whereas the layers below the MgO barrier were patterned to a circular shape with a diameter of 180 μm. Circular shapes were selected to avoid the in-plane shape anisotropy. The patterned devices were annealed at 350 °C for 1 h under a magnetic field of 0.7 T. The resistance-area product values in the parallel magnetization configuration (RA_p) of the devices were 20–200 kΩ μm^2 (A = 1,256 μm^2). Despite the variation in the RA_p value, which was due to batch-to-

batch variation and non-uniformity within the substrate of the MgO thickness and quality, the TMR ratio was approximately constant at 180%.

Figure 2(b) shows the expected magnetization (**m**) configuration of the FM layers of the TMR device under zero external magnetic field (H). $\mathbf{m}_{PL2}$ was pinned at an angle of θ_{IEC} from $\mathbf{m}_{PL1}$, and $\mathbf{m}_{FL}$ was stabilized along the same direction as $\mathbf{m}_{PL2}$. H was applied along the x direction. Figure 2(c) shows the TMR curves of these devices. For the pure Ru spacer, the TMR ratio was 0 at $H_x = 0$, indicating a parallel configuration between the $\mathbf{m}_{FL}$ and $\mathbf{m}_{RL}$. Thus, the type of the IEC through the pure Ru spacer was AFM. Rotation of $\mathbf{m}_{FL}$ was observed at $\mu_0 H_x$ of approximately 8 mT, which is the strength of the orange-peel FM coupling through the AgSn spacer. The TMR ratio at $H_x = 0$ changed for different Fe concentrations in the RuFe spacer. Thus, the magnetization angle between the FL and RL was controlled by the noncollinear IEC through the RuFe spacer. However, these devices exhibited pronounced magnetic hysteresis, rendering them unsuitable for magnetic sensor applications. The coercivity (H_c) of the TMR curve for the $Ru_{37}Fe_{63}$ spacer was 0.23 mT.

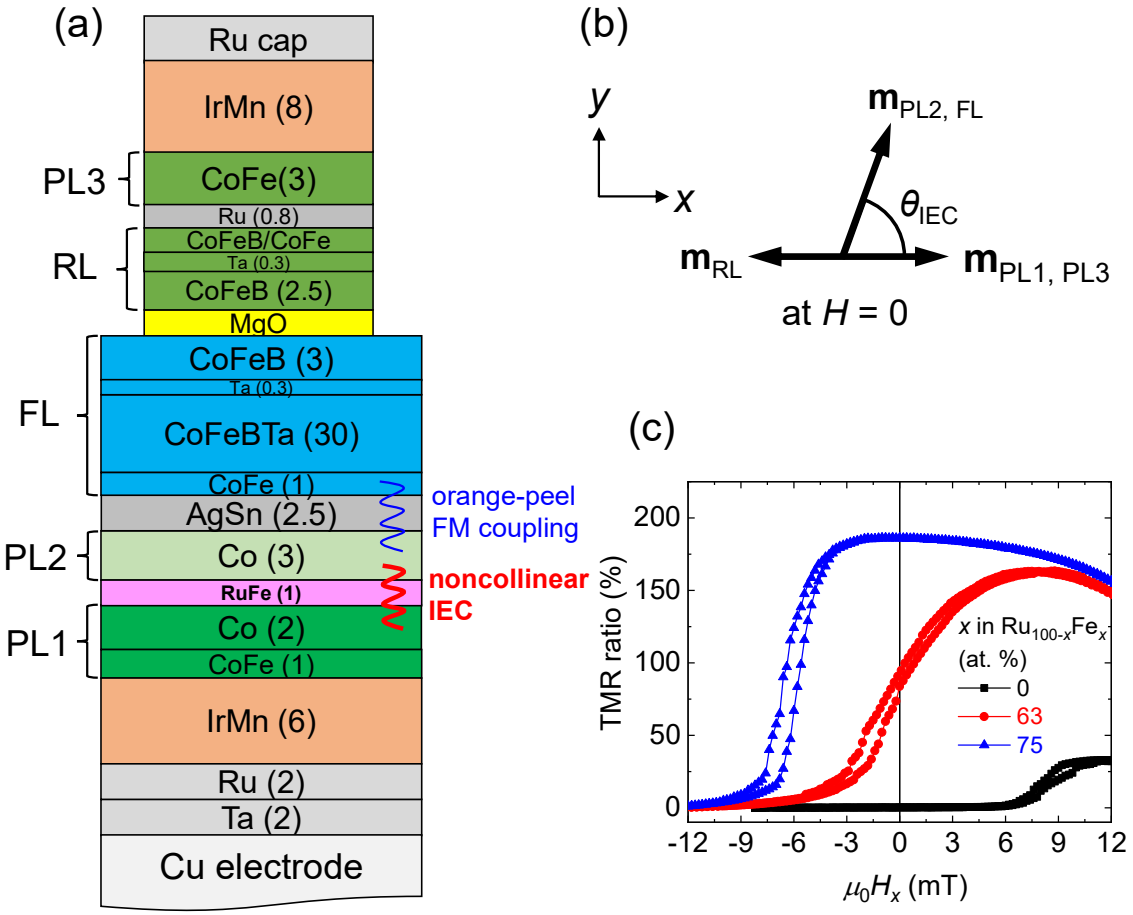

FIG. 2. (a) TMR spin-valve structure with FL whose magnetization direction is stabilized along a noncollinear direction with respect to the pinning direction by the noncollinear IEC through the RuFe spacer. (b) Magnetization (**m**) configuration of the FM layers of the spin-valve under a zero external magnetic field (*H*). (c) TMR curves of the devices with variation in Fe concentration in the RuFe spacer. *H* was applied along the *x* direction.

Note that annealing process under a magnetic field induces uniaxial magnetic anisotropy in FM layers. Therefore, in the present spin-valve devices, the magnetization process of FL is governed by three factors: unidirectional anisotropy, uniaxial anisotropy, and external *H*. Trial and error of the annealing process revealed that the uniaxial anisotropy induced in the tilted angle from the direction of *H* significantly reduced the magnetic hysteresis of the TMR

curves. The reason for this has not yet been elucidated. Further, the shape of the TMR curve was highly dependent on the direction of the uniaxial anisotropy. To understand this behavior, we performed numerical simulations of the TMR curve in the single magnetic domain regime using the Stoner-Wohlfarth model.

Figure 3(a) shows the configuration of the in-plane magnetization of the FM layers and the directions of the magnetic anisotropies of the FL. The unidirectional and uniaxial anisotropies were induced at angles of θ_{ud} and θ_{ua}, respectively, with respect to $\mathbf{m}_{PL1}$ which was pinned along the $+x$ direction. This configuration of the two types of magnetic anisotropies was achieved by the annealing process shown in Fig. 3(b). First, the devices were annealed at 350 °C under a magnetic field at θ_{ua}, which induced a uniaxial anisotropy parallel to this direction and also crystallized the CoFeB/MgO interfaces. Thereafter, the temperature was lowered to 220 °C, which was above the blocking temperature of the IrMn layer (approximately 200 °C). The magnetic field direction was then changed to the $+x$ direction ($\theta = 0°$), and the temperature was lowered to room temperature, which pinned $\mathbf{m}_{PL1}$ and $\mathbf{m}_{PL3}$ along this direction.

In addition, the unidirectional anisotropy of the FL has two equivalent directions at θ_{ud} clockwise and counterclockwise from $\mathbf{m}_{PL1}$, as shown in Fig. 3(a). The FL magnetization state realized depends on the history of application of external H to the device. For simplicity, we considered only the unidirectional anisotropy counterclockwise from $\mathbf{m}_{PL1}$, which can be selected by applying H along the $+y$ direction, hereafter referred to as a "set field", prior to the TMR measurement with sweeping H_x. The angle (θ_{FL}) between the FL magnetization and H_x was calculated by minimizing the total magnetic energy, considering the Zeeman energy, exchange bias, annealing-induced uniaxial anisotropy, AFM and noncollinear IEC through the Ru and RuFe spacers, respectively, and the orange-peel FM coupling through the AgSn spacer. The calculation details are provided in the Supplementary Material.

Figure 3(c) shows the simulated TMR curves for a constant θ_{ud} of 120° and θ_{ua} = 0–120°. The TMR curve shape was strongly dependent on θ_{ua}, and the highest value of sensitivity, defined by $\frac{1}{R}\frac{dR}{dH}$, at $H_x = 0$ was obtained for θ_{ua} = 30°. Figure 3(d) shows the contour plot of the sensitivity at $H_x = 0$ for θ_{ud} and θ_{ua}, providing the choice of the values of θ_{ud} and θ_{ua} to obtain high sensitivity. Figures 3(e) and (f) show the experimental TMR curves for the 1-nm-thick $Ru_{40}Fe_{60}$ and $Ru_{35}Fe_{65}$ spacers, respectively. The angles of the magnetic anisotropies were θ_{ud} ~130° and θ_{ua} = 40° for the $Ru_{40}Fe_{60}$ spacer, and θ_{ud} ~120° and θ_{ua} = 120° for the $Ru_{35}Fe_{65}$ spacer. θ_{ud} was estimated by fitting the *M–H* curves (not shown here), and θ_{ua} was controlled by the annealing process. Compared to the device with $\theta_{ua} = 0$, which exhibited $\mu_0 H_c$ = 0.23 mT [Fig. 2(c)], these device with $\theta_{ua} \neq 0$ showed significantly reduced hysteresis: $\mu_0 H_c \sim 0.02$ mT for the $Ru_{40}Fe_{60}$ spacer and $\mu_0 H_c \sim 0$ mT for the $Ru_{35}Fe_{65}$ spacer [the insets of Figs. 3(e) and (f), respectively], indicating that a single magnetic domain structure was obtained for $\theta_{ua} \neq 0$. For the $Ru_{40}Fe_{60}$ spacer, the highest sensitivity state (21 %/mT) was obtained at $H_x = 0$, which is preferred for magnetic sensor applications. On the other hand, the device with the $Ru_{35}Fe_{65}$ spacer exhibited a relatively low sensitivity at $H_x = 0$ (14 %/mT). The trend of the sensitivity at $H_x = 0$ of these devices was consistent with the simulated results shown in Fig. 3(d). However, magnetic hysteresis cannot be simulated in the single-domain regime. Thus, the reason why tilting the uniaxial anisotropy axis of FL away from the pinning and *H* directions significantly reduced the hysteresis of the *R–H* curve is an open question.

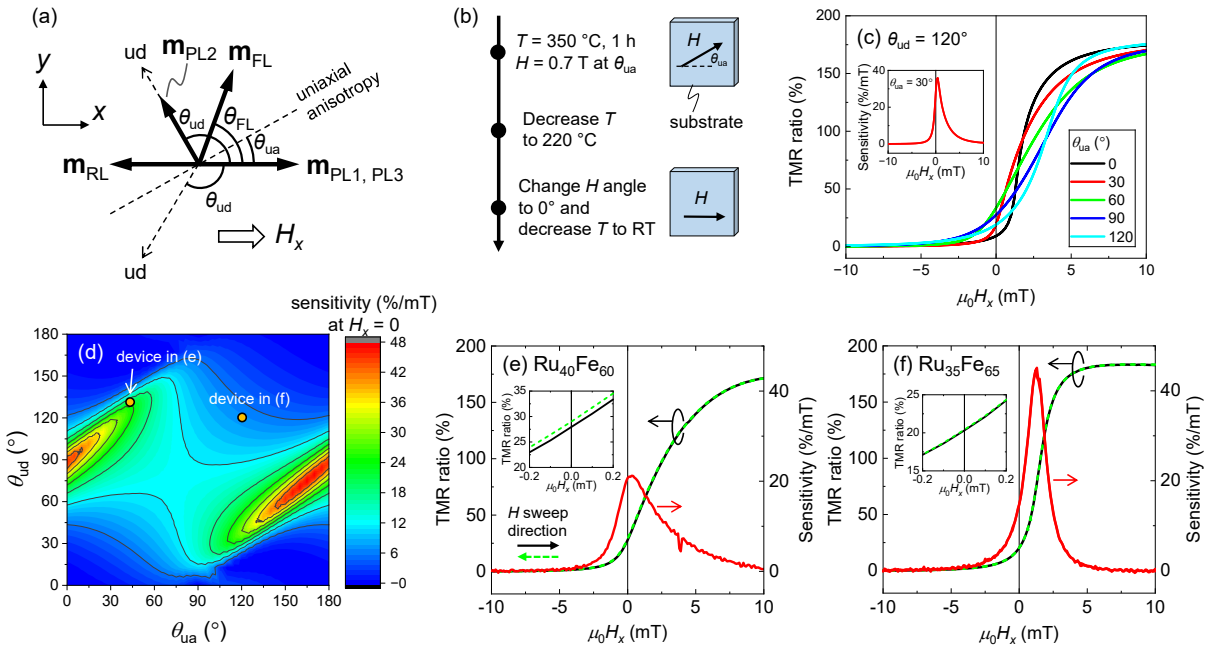

FIG. 3. (a) Configuration of the magnetizations (**m**) of the FM layers of the spin-valve device. The unidirectional anisotropy has two equivalent directions with respect to $\mathbf{m}_{PL1}$, indicated as the dashed arrows labeled as "ud". θ_{ua} and θ_{ud} are the angles between the easy axes of the uniaxial and unidirectional anisotropies, respectively, and $\mathbf{m}_{PL1}$. (b) Annealing process to obtain the anisotropy configuration in (a). (c) Simulated TMR curves for θ_{ud} = 120° and θ_{ua} = 0–120°. The inset shows the sensitivity curve for θ_{ua} = 30°. (d) Contour plot of sensitivity at H_x = 0 for θ_{ua} and θ_{ud}. (e) and (f) Experimental TMR and sensitivity curves with 1-nm-thick $Ru_{40}Fe_{60}$ and $Ru_{35}Fe_{65}$ spacers, respectively. The insets show the same TMR curves in a small field range.

Next, we discuss the effects of the two possible directions of unidirectional anisotropy on the shape of the TMR curve. Figure 4(a) shows the magnetization configuration diagram. After applying a set field of $H_y > 0$, $\mathbf{m}_{FL}$ stabilizes to the state indicated by the blue counterclockwise arrow from $\mathbf{m}_{PL1}$ owing to the balance of the uniaxial and unidirectional anisotropies. Similarly, after $H_y < 0$ is applied, $\mathbf{m}_{FL}$ stabilizes to the state indicated by the red arrow. The shape of the TMR curve changes depending on the direction of the set field, as

confirmed experimentally and shown in Fig. 4(b). This device was fabricated with a $Ru_{35}Fe_{65}$ (1 nm) spacer with $\theta_{ud} \sim \pm 120°$ and $\theta_{ua} = 60°$. First, we applied a positive set field H_y and measured the R–H_x curve for $H_y = 0$. The TMR curve plotted in blue in Fig. 4(b) exhibited the highest sensitivity and relatively good linearity at $H_x = 0$, indicating that the angle between $\mathbf{m}_{FL}$ and $\mathbf{m}_{RL}$ at $H_x = 0$ was approximately 90°. After negative H_y was applied, the TMR curve changed its shape, as shown in red, because $\mathbf{m}_{FL}$ was stabilized along a different direction from that of positive H_y, as shown schematically depicted in Fig. 4(a). When positive H_y was applied again, the TMR curve shown by the dashed green curve was identical to that following the first positive H_y (blue). Therefore, the stabilization of $\mathbf{m}_{FL}$ along two directions by unidirectional anisotropy and the TMR curve are reversible. For magnetic sensors, TMR curves with a high sensitivity at $H_x = 0$ and good linearity are preferred, which is the case for the positive set field for this device. However, the presence of another magnetization energy minimum requires care not to expose the sensor device to an unexpectedly large magnetic field along the y direction.

The present devices achieve essentially the same function as the sensors with soft-pinned FLs,[12,13,20,21] in terms of linear R–H curves with negligible hysteresis. The soft-pinned FL sensors obtain unidirectional FL anisotropy orthogonal to the RL magnetization by two-step annealing for two AFM layers with different blocking temperatures, e.g., PtMn and IrMn layers. The strength of the FL anisotropy field is controlled by the thickness of the ultrathin dusting layer, typically with Ru, inserted between the AFM layer and the FL. On the other hand, the present devices achieve a noncollinear magnetization configuration between the FL and RL by exchange bias transferred via a noncollinear IEC through the RuFe spacer. The FL anisotropy field is controlled by the strength of the orange-peel FM coupling through the thickness of the AgSn nonmagnetic spacer. These two types of sensor designs may have different advantages and challenges depending on the required sensor characteristics such as sensitivity and dynamic

range. Therefore, for specific applications, various technical and economic aspects such as sensing characteristics, reliability, manufacturability, and cost must be evaluated.

In summary, we have developed a TMR sensor structure wherein the magnetization of the FL is stabilized in the single-domain regime in an arbitrary direction by a noncollinear IEC through a RuFe spacer. The strength of the magnetic stabilization field of the FL is controlled by orange-peel FM coupling through a nonmagnetic spacer, such as AgSn. Further, the uniaxial magnetic anisotropy induced by magnetic field annealing facilitate the determination of the shape of the TMR curve and its magnetic hysteresis. By controlling the directions of the noncollinear IEC and uniaxial magnetic anisotropy, TMR sensor devices with high sensitivity under a zero magnetic bias field and negligible magnetic hysteresis can be obtained, which are promising for various magnetic sensing applications.

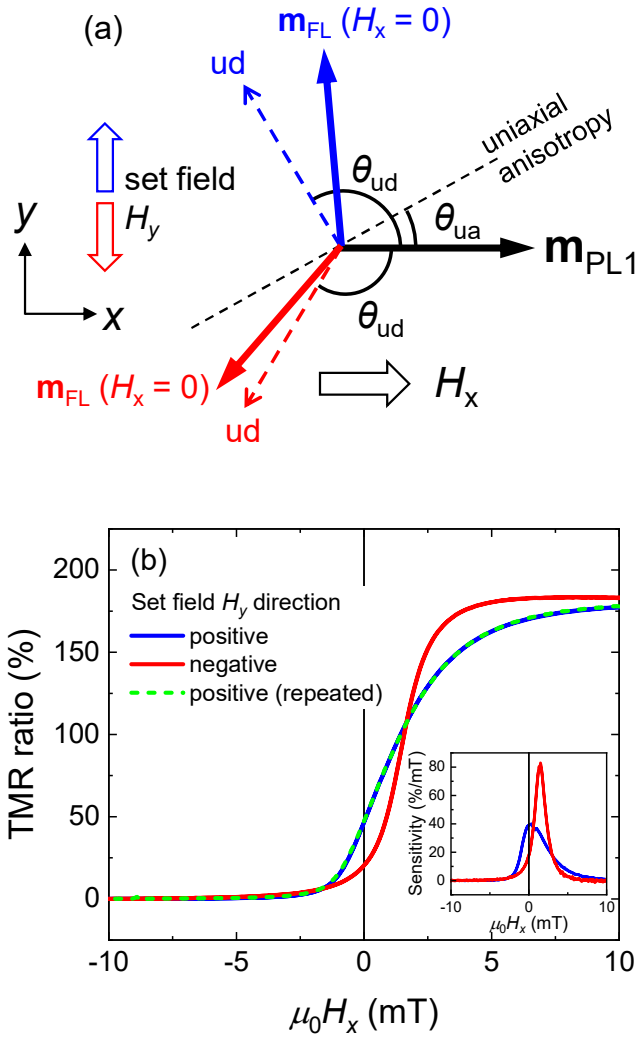

FIG. 4. (a) Magnetization configuration depending on the direction of set field (H_y). The blue and red arrows indicate $\mathbf{m}_{FL}$ at H_x = 0 after applying positive and negative H_y, respectively. (b) Experimental TMR curves along two directions of set field (θ_{ud} ~ ±120° and θ_{ua} = 60°).

Acknowledgement

We thank Hiroshi Imamura (National Institute of Advanced Industrial Science and Technology) for valuable discussions.

Supplementary material

Refer to the supplementary material for details of the *R*-*H* curve simulations and the hysteresis of the device shown in Fig. 4(b).

Data Availability Statement

The data supporting the findings of this study are available from the corresponding author upon reasonable request.

Conflict of interest

The authors have no conflict of interest regarding the publication of this article.

References

[1] B. Dieny, V.S. Speriosu, S.S.P. Parkin, B.A. Gurney, D.R. Wilhoit, and D. Mauri, Phys. Rev. B **43**, 1297 (1991).

[2] S.S.P. Parkin, N. More, and K.P. Roche, Phys. Rev. Lett. **64**, 2304 (1990).

[3] S.S.P. Parkin, R. Bhadra, and K.P. Roche, Phys. Rev. Lett. **66**, 2152 (1991).

[4] S.S.P. Parkin, Phys. Rev. Lett. **67**, 3598 (1991).

[5] S.S.P. Parkin and D. Mauri, Phys. Rev. B **44**, 7131 (1991).

[6] R.S. Beach, M. Pinarbasi, and M.J. Carey, J. Appl. Phys. **87**, 5723 (2000).

[7] Z.R. Nunn, C. Abert, D. Suess, and E. Girt, Sci. Adv. **6**, eabd8861 (2020).

[8] Z.R. Nunn, J. Lisik, P. Omelchenko, S. Koraltan, C. Abert, D. Suess, and E. Girt, J. Appl. Phys. **133**, 123901 (2023).

[9] C. Abert, S. Koraltan, F. Bruckner, F. Slanovc, J. Lisik, P. Omelchenko, E. Girt, and D. Suess, Phys. Rev. B **106**, 054401 (2022).

[10] J. Besler, S. Myrtle, and E. Girt, J. Magn. Magn. Mater. **585**, 171109 (2023).

[11] X. Liu, C. Ren, and G. Xiao, J. Appl. Phys. **92**, 4722 (2002).

[12] D. Wang, J. Daughton, C. Nordman, P. Eames, and J. Fink, J. Appl. Phys. **99**, 08H703 (2006).

[13] B. Negulescu, D. Lacour, F. Montaigne, A. Gerken, J. Paul, V. Spetter, J. Marien, C. Duret, and M. Hehn, Appl. Phys. Lett. **95**, 112502 (2009).

[14] A. V. Silva, D.C. Leitao, J. Valadeiro, J. Amaral, P.P. Freitas, and S. Cardoso, EPJ Appl. Phys. **72**, 10601 (2015).

[15] Y. Lu, R.A. Altman, A. Marley, S.A. Rishton, P.L. Trouilloud, G. Xiao, W.J. Gallagher, and S.S.P. Parkin, Appl. Phys. Lett. **70**, 2610 (1997).

[16] P. Wisniowski, J. Wrona, T. Stobiecki, S. Cardoso, and P.P. Freitas, IEEE Trans. Magn. **48**, 3840 (2012).

[17] P. Wisniowski, M. Dabek, J. Wrona, S. Cardoso, and P.P. Freitas, J. Appl. Phys. **122**, (2017).

[18] K. Fujiwara, M. Oogane, S. Yokota, T. Nishikawa, H. Naganuma, and Y. Ando, J. Appl. Phys. **111**, 07C710 (2012).

[19] D. Kato, M. Oogane, K. Fujiwara, T. Nishikawa, H. Naganuma, and Y. Ando, Appl. Phys. Express **6**, 103004 (2013).

[20] R. Ferreira, E. Paz, P.P. Freitas, J. Wang, and S. Xue, IEEE Trans. Magn. **48**, 3719 (2012).

[21] J.Y. Chen, J.F. Feng, and J.M.D. Coey, Appl. Phys. Lett. **100**, 142407 (2012).

[22] M. Oogane, K. Fujiwara, A. Kanno, T. Nakano, H. Wagatsuma, T. Arimoto, S. Mizukami, S. Kumagai, H. Matsuzaki, N. Nakasato, and Y. Ando, Appl. Phys. Express **14**, 123002 (2021).

[23] E.E. Fullerton and S.D. Bader, Phys. Rev. B **53**, 5112 (1996).

[24] P.D. Kulkarni, T. Nakatani, T. Sasaki, and Y. Sakuraba, J. Appl. Phys. **129**, 213901 (2021).

[25] J.C.S. Kools, W. Kula, D. Mauri, and T. Lin, J. Appl. Phys. **85**, 4466 (1999).

[26] T. Nakatani, H. Suto, P.D. Kulkarni, H. Iwasaki, and Y. Sakuraba, Appl. Phys. Lett. **121**, 192406 (2022).